A Low-Cost *Ka*-Band Circularly Polarized Passive Phased-Array Antenna for Mobile Satellite Applications

Hussam Al-Saedi, *Student Member, IEEE*, Suren Gigoyan, Wael M. Abdel-Wahab, Ardeshir Palizban, Aidin Taeb, *Member, IEEE*, Ahmad Ehsandar, Elizaveta Nenasheva, and Safieddin Safavi-Naeini, *Life Fellow, IEEE*

***Abstract*— This paper presents a low-profile, high-performance, and low-cost *Ka*-band circularly polarized (CP) passive phased-array antenna (PAA) system. A 1 × 4 passive subarray operating at the *Ka*-band frequency band is investigated, developed, and tested as a possible building block for mobile satellite communication systems. In particular, a CP antenna integrated with a high-performance passive phase shifter is presented and experimentally verified. A new low-cost and low-profile magnetic actuator is proposed to precisely control the phase state of the phase shifter. A 3-D printed polymer package is utilized to enclose the phase shifter and reduce the environmental effects. The proposed CP passive PAA achieves high-performance right-hand CP radiation with high cross-polarization discrimination over a wide scan angle from 0° to ±38° over the frequency band (29.5–30.5 GHz). An axial ratio (AR) < 3 dB is demonstrated over the entire scanning range. Moreover, the measured radiation efficiency is 60% at boresight. The gain drops by 1 dB at ±38° scanning angles.**

***Index Terms*— Circularly polarized (CP) antenna, millimeter-wave (mm-W) phased-array antenna (PAA), phase shifter, satellite mobile communication.**

I. Introduction

AS THE demand for higher data rates increases, wireless technologies (e.g., satellite communications, 5G, and automotive radar) are migrating toward millimeter-wave (mm-W) frequencies to utilize the large available frequency bandwidth over this frequency band (e.g., *Ka*-band) [1]–[13]. A phased-array antenna (PAA) can offer a low-profile conformal solution with fast beam scanning, as compared to the reflector antenna [14]. These unique features are essential for emerging *Ka*-band mobile satellite communication, which requires a low-profile robust antenna system to dynamically track the satellite when the terminal moves and maneuvers [14]–[17]. The cost and complexity of active feed circuits have seriously limited the deployment of active PAA in mass market applications. A wideband passive PAA can offer an attractive low-cost alternative for a wide range of emerging mm-W communication systems [18]–[26]. Such antenna systems are made of passive components, (antennas, phase shifters, and passive feeding networks), to reduce the power consumption, cost, and complexity. Furthermore, a single passive PAA made of reciprocal components can be utilized as both a transmitter and receiver. In order to build such systems, a high-performance antenna and phase shifter must be developed and integrated. The antenna element should be simple and have a wide operating frequency band. Moreover, it would be required to demonstrate a high cross-polarization discrimination over a wide angular beamwidth to sustain a high-quality data link and avoid undesired interferences. In addition, the phase shifter must have a low insertion loss (IL) variation over the operating frequency range to eliminate the necessity for costly variable gain amplifiers. The phase shifter needs to provide a continuous phase shift of 360°, so the beam can be steered to any direction in space precisely and quickly. A wideband phase shifter using a relatively low dielectric tapered slab to perturb the propagating electromagnetic wave in a transmission line is reported in [18]–[26]. This phase shifter was incorporated into a linear antenna array to develop a wideband passive PAA. A piezoelectric transducer (PET) was used to control this phase shifter. However, the passive PAAs presented in [18]–[26] have several drawbacks and limitations. A large dielectric slab ($>\lambda_o$) is required to realize a 360° phase shift. Therefore, the interelement spacing will be $\gg 0.5\ \lambda_o$ in one plane of the 2-D PAA, which leads to the appearance of the grating lobe when the beam is steered in that particular plane. Accordingly, this method is limited to only linear (1-D) phase-array configuration. The PET requires a high voltage to operate, necessitating a high voltage power

Manuscript received November 19, 2017; revised August 6, 2018; accepted October 14, 2018. Date of publication October 31, 2018; date of current version January 16, 2019. This work was supported in part by the Iraqi Ministry of Higher Education and Scientific Researche, in part by C-COM Satellite Systems Inc., and in part by the National Science and Engineering Research Council of Canada. *(Corresponding author: Hussam Al-Saedi.)*

H. Al-Saedi is with the Department of Communication Engineering, University of Technology, Iraq, Baghdad 10066, Iraq, and also with the Department of Electrical and Computer Engineering, University of Waterloo, Waterloo, ON N2L 3G1, Canada (e-mail: hhalsaed@uwaterloo.ca).

S. Gigoyan, A. Palizban, A. Taeb, and S. Safavi-Naeini are with the Department of Electrical and Computer Engineering, University of Waterloo, Waterloo, ON N2L 3G1, Canada (e-mail: gigoyan@uwaterloo.ca; apalizban@uwaterloo.ca; ataeb@uwaterloo.ca; safavi@uwaterloo.ca).

W. M. Abdel-Wahab and A. Ehsandar are with C-COM Satellite Systems Inc., Ottawa, ON K1B 3V7, Canada, and also with the Department of Electrical and Computer Engineering, University of Waterloo, Waterloo, ON N2L 3G1, Canada (e-mail: wmabdelw@uwaterloo.ca; aehsandar@uwaterloo.ca).

E. Nenasheva is with Ceramics Co. Ltd., Private R&D Company, Saint Petersburg 194223, Russia (e-mail: ramics1990@gmail.com).

Color versions of one or more of the figures in this paper are available online at http://ieeexplore.ieee.org.

Digital Object Identifier 10.1109/TAP.2018.2878335

supply be a component of a large PAA. The PETs used in these structures are bulky. Furthermore, no packaging structure has been presented to-date to protect such systems against environmental effects. In [18]–[26], since a single tapered dielectric slab has been used to control the phase state of the antenna elements, the beam of these phased arrays can only be steered in one direction off-boresight, which is the main drawback of such structures. To steer the beam in two directions, a second complementary dielectric slab must be used that adds more complexity and increases the size of the phased array. This type of PAA is prone to large pointing errors due to warpage of the printed circuit board (PCB); as a result, any local surface defect can affect the progressive phase state of that specific antenna element and there is no way to correct this phase error. This lack of independence can lead to serious difficulties in phase calibration. It should be noted that none of the reported configurations has been presented in a low-profile and packaged form. Moreover, to the best of the authors' knowledge, a circularly polarized (CP) passive PAA has not been presented in the literature employing this beam scanning technique.

The objective of this paper is to investigate enabling technologies and develop a proof-of-concept prototype for a low-cost and low-profile compact CP passive PAA for mm-W applications (*Ka*-band systems specifically). First, an aperture-coupled CP antenna is designed to operate at *Ka*-band (29–31 GHz) with a wide angular axial ratio (AR) beamwidth. A low-cost and high-performance compact phase shifter consisting of a grounded coplanar waveguide (GCPW) line with a high dielectric material slab is integrated with the antenna to realize the proposed CP passive PAA. Furthermore, a novel low-profile actuation method is presented with a 3-D printed enclosure to avoid the bulky PET structure. The remainder of this paper is divided into three main sections that describe the antenna element, phase shifter, and CP passive PAA, respectively.

II. Circularly Polarized Antenna

A. Circularly Polarized Ka-Band Aperture-Coupled Antenna Element

A CP PAA with a wide scanning angle requires an antenna element with wide angular AR < 3-dB beamwidth. In addition, the interelement separation must be $\leqslant 0.5\ \lambda_o$ to avoid the grating lobe effect. In this paper, a novel CP patch antenna element based on aperture-coupled excitation is proposed for low-cost *Ka*-band applications. The proposed antenna design was inspired by the work presented in [27]. The antenna structure consists of three metal layers (M1, M2, and M3) as shown in Fig. 1(a) and (b). An elliptical microstrip patch antenna (M1) is etched on the top substrate with a major axis of $2R_1$ and a minor axis of $2R_2$, where the two values are chosen to achieve a wide impedance bandwidth. The middle metal layer (M2) forms the ground plane and contains a square ring slot (L-shaped) to degenerate two orthogonal modes with equal amplitudes and a 90° phase difference. The slot ring has six arms with lengths labeled (L_{s1}–L_{s6}) and a slot gap of S. With this slot configuration, two orthogonal transverse electric fields can be degenerated in the X and Y directions over the

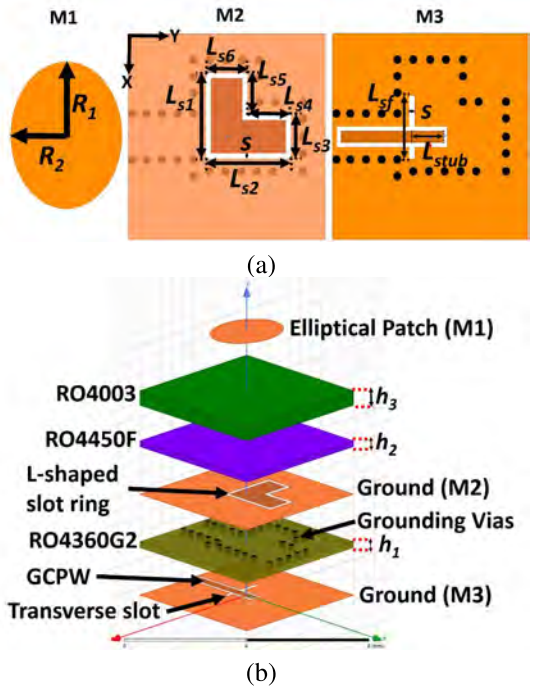

Fig. 1. Proposed CP antenna structure. (a) Metal layers. (b) 3-D exploded view.

slot gap. The length of the arms L_{s1} and L_{s2} are chosen to ensure the square ring slot has an electrical length of λ at the resonance frequency, and the arms L_{s3}, L_{s4}, L_{s5}, and L_{s6} are chosen to excite two orthogonal modes with a 90° phase difference. The slot is coupled to a GCPW line (M3) that is etched at the backside of the bottom substrate through a series transverse slot. The ground size of the antenna element is 5×5 mm^2($0.5\ \lambda_o \times 0.5\lambda_o$) at 30 GHz. RO4003 substrate ($\varepsilon_r = 3.55$, $\tan_\sigma = 0.0027$) is used to design the radiating patch and RO4360G2 substrate ($\varepsilon_r = 6.15$, $\tan_\sigma = 0.0038$) is used to design the GCPW feed line. In addition, RO4450F substrate ($\varepsilon_r = 3.52$, $\tan_\sigma = 0.004$) is used to bond the above-mentioned substrates. The elliptical patch has two dominant resonance modes, which are $TM11^{e,o}$ odd and even. The resonance frequency of these modes can be calculated from (1) to (5) [28]

$$f_{11}^{o,e} = \frac{15}{\pi R_{1eff}\sqrt{\varepsilon_r}}\sqrt{q_{11}^{o,e}}. \tag{1}$$

$$e = \sqrt{1-(\frac{R_2}{R_1})^2}. \tag{2}$$

$$q_{11}^{o} = -0.0063e + 0.38316e^2 - 1.1351e^3 + 5.2229e^4. \tag{3}$$

$$q_{11}^{e} = -0.0049e + 3.7888e^2 - 0.7278e^3 + 2.314e^4. \tag{4}$$

$$R_{1eff} = \left[R_1 + \frac{hR_1}{0.3525\pi\varepsilon_r} ln\left(\frac{R_1}{2h}\right) + (1.41\varepsilon_r + 1.77) + \frac{h}{R_1}(0.268\varepsilon_r + 1.65)\right]^{\frac{1}{2}}. \tag{5}$$

B. Simulation Results for Proposed Antenna Element

A commercial full-wave simulator from ANSYS (HFSS 18.2) was used to analyze and optimize the

TABLE I
OPTIMIZED PARAMETERS OF CP ANTENNA (millimeter)

Parameter	R_1	R_2	L_{s1}	L_{s2}	L_{s3}	L_{s4}	L_{s5}
Dimension	1.345	1.06	2.1	2.17	1.07	1.1	1.025
Parameter	L_{s6}	S	L_{sf}	L_{stub}	h_1	h_2	h_3
Dimension	1.072	0.14	1.525	0.8	0.203	0.203	0.508

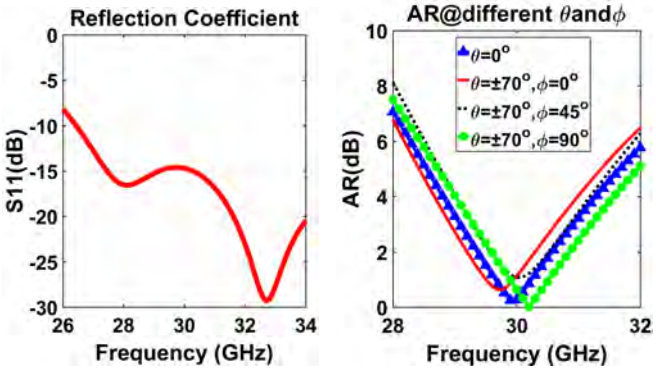

(a) (b)

Fig. 2. Simulated reflection coefficient and AR. (a) S_{11} (dB). (b) AR (dB) for $\phi = 0°$, 45°, and 90°; and $\theta = 0°$ and $\pm 70°$.

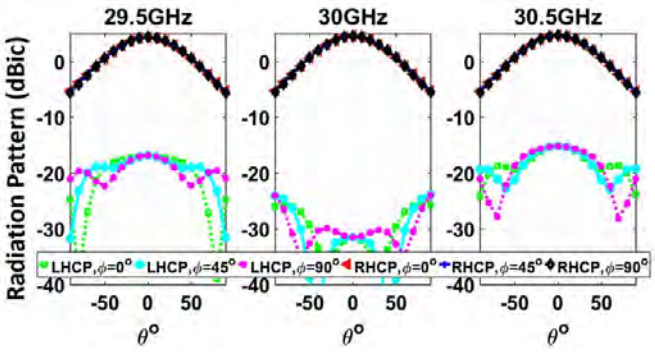

Fig. 3. Simulated radiation patterns at 29.5, 30, and 30.5 GHz for $\phi = 0°$, 45°, and 90°.

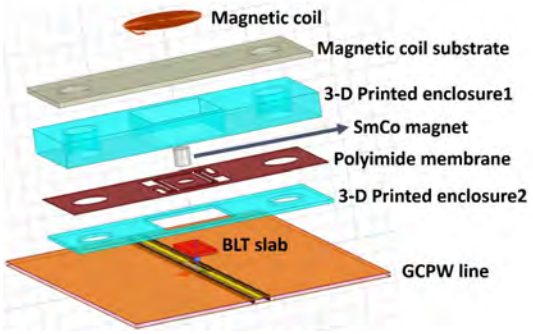

Fig. 4. Exploded 3-D view of phase shifter with magnetic actuator and 3-D printed enclosure.

antenna parameters. An extensive parametric study was conducted on the antenna's parameters to examine their impacts on the overall antenna's performance. It was found that the slot arms L_{s4}, L_{s5}, and the eccentricity of the elliptical patch, e, are the most critical parameters affecting the purity of the circular polarization pattern over a wide angular beamwidth. The major axis $2R_1$, the slot arms L_{s1}, L_{s2}, the feeding point, and the length of the transverse slot L_{sf} were found to be mainly responsible for the impedance bandwidth. The antenna parameters were optimized by using the HFSS optimization tool, the goal being to achieve the optimum AR and impedance matching over the operating frequency band (i.e., 29–31 GHz). The optimized parameters of the antenna are given in Table I. Using the state-of-the-art multilayer fabrication technology, high-quality planar antennas and feed circuits can be realized with the dimensional accuracy better than 20 μm. Extensive full-wave sensitivity analysis (not shown for brevity) have been conducted on the proposed antenna with ± 20 μm variation from the nominal values of some critical design parameters (e.g., R_1, R_2, L_{s1}, L_{s4}, S, L_{sf}, and L_{stub}). Simulation results reveal that the proposed antenna is not highly sensitive to parameters variation within the range of the fabrication tolerances. The simulation results show an impedance bandwidth ($S_{11} < -10$ dB) of almost 8 GHz centered at 30 GHz. The two resonances of the elliptical patch appear at 28 and 32.75 GHz, as shown in Fig. 2(a). The proposed antenna shows an AR < 3 dB bandwidth of 1.8 GHz (6%) centered at 30 GHz at the boresight and an AR bandwidth of 1.3 GHz over an angular beamwidth from $-70°$ to $+70°$ off-boresight, as shown in Fig. 2(b). These results demonstrate that the antenna satisfies most of the stringent *Ka*-band system requirements in terms of the reflection coefficient, size, and AR and angular beamwidths. It has a 5 dBic gain over the operating frequency, with an almost symmetrical pattern over the azimuth angles (ϕ); moreover, it shows a cross-polarization discrimination better than 35 dB at 30 GHz, as shown in Fig. 3.

1) Tables: Data charts which are typically black and white, but sometimes include color.

III. LOW-PROFILE MILLIMETER-WAVE PHASE SHIFTER

A new low-profile and high-performance phase shifter is proposed in this paper. The phase shifter was inspired by the work presented in [29]. It consists of a GCPW line, a high dielectric slab, a magnetic actuator, and a 3-D printed packaging structure. The proposed phase shifter is implemented in a PCB technology that allows for direct integration with the antenna; therefore, no wire bonding or ball grid arrays are required. The GCPW line is designed on RO4360G2 dielectric substrate with an ($\varepsilon_r = 6.15$, $\tan_\sigma = 0.0038$), and a thickness of $h_1 = 0.2032$ mm with a 50 Ω impedance at the input–output. The dielectric slab is made of barium lanthanide tetratitanates (BLT; BaLn2Ti4O12), and has a length of $L_{BLT} = 4$ mm, a width of $W_{BLT} = 1.5$ mm, a height of $h_{BLT} = 0.2$ mm, an $\varepsilon_r = 100$, and a dielectric loss of $\tan_\sigma = 0.01$ at 30 GHz [30], [31]. The BLT slab is placed on top of the GCPW line, and the magnetic actuator is utilized to control the position of the BLT slab. This allows a tunable and continuous phase to be realized. An exploded view of the proposed phase shifter is shown in Fig. 4.

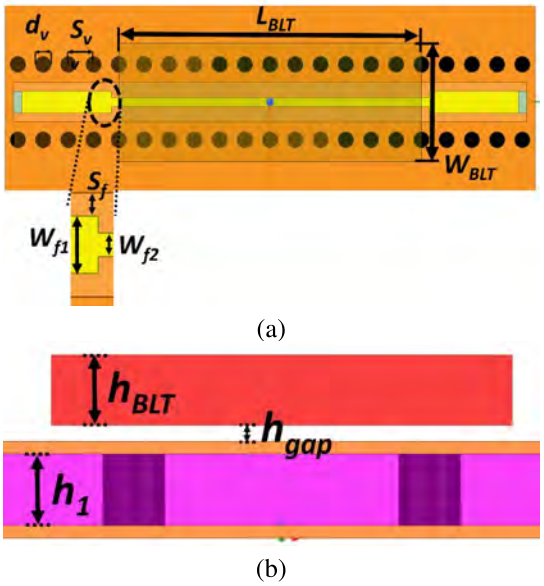

Fig. 5. Proposed phase shifter circuit. (a) Top view. (b) Side view.

TABLE II
OPTIMIZED PARAMETERS OF PHASE SHIFTER (millimeter)

Parameter	W_{f1}	S_f	L_{BLT}	W_{BLT}	h_{BLT}
Dimension	0.28	0.11	4	1.5	0.2
Parameter	W_{f2}	d_v	S_v	h_1	-
Dimension	0.11	0.203	0.5	0.203	-

A. Simulation Results for Proposed Phase Shifter

The GCPW line, shown in Fig. 5(a), has a linewidth of $W_{f1} = 0.28$ mm and a gap size of $S_f = 0.11$ mm at the input and output of the phase shifter. The existence of the BLT slab reduces the GCPW line impedance, so impedance matching is introduced on the GCPW part below the BLT slab. Impedance matching is realized by decreasing the width of the GCPW line from 0.28 mm to $W_{f2} = 0.11$ mm; therefore, the proposed phase shifter shows an $S_{11} < -10$ dB for all the phase states over the operating frequency band. The proposed phase shifter has a wide operating bandwidth as was demonstrated in [29] and [30]; however, for this prototype, it was designed and tested over the operating frequency band of the CP antenna (i.e., 29–31 GHz centered at 30 GHz), and its optimized dimensions are listed in Table II.

Simulations were performed to optimize the phase shifter and to calculate the actuation height required to realize $> 360°$ phase shift. As the BLT slab moves, an air gap (h_{gap}) is created between the GCPW line and the BLT slab. Most of the electromagnetic energy propagates in the air gap, which behaves as an adjustable waveguide. As a result, the phase shifter shows a low IL and *more importantly minimal IL variation* as the phase shift changes. Simulations showed that to realize a 360° phase shift, the air gap h_{gap} should vary between 1 and 45 μm as shown in Fig. 6(a). From this figure, it can be observed that the phase response of S21 varies exponentially with h_{gap}. A small h_{gap}'s contributes more significantly to the phase shift than large gaps. Moreover, the proposed phase shifter demonstrates an $S_{11} < -10$ dB over the operating frequency band (29–31 GHz) for all h_{gap} values. Similarly, it depicts very low IL for the same frequency bandwidth. The simulation results show an average IL of 0.95 dB at 30 GHz with an exceptionally low IL variation of less than ± 0.5 dB over the entire range of phase shift. The simulated S-parameters are shown in Fig. 6(b).

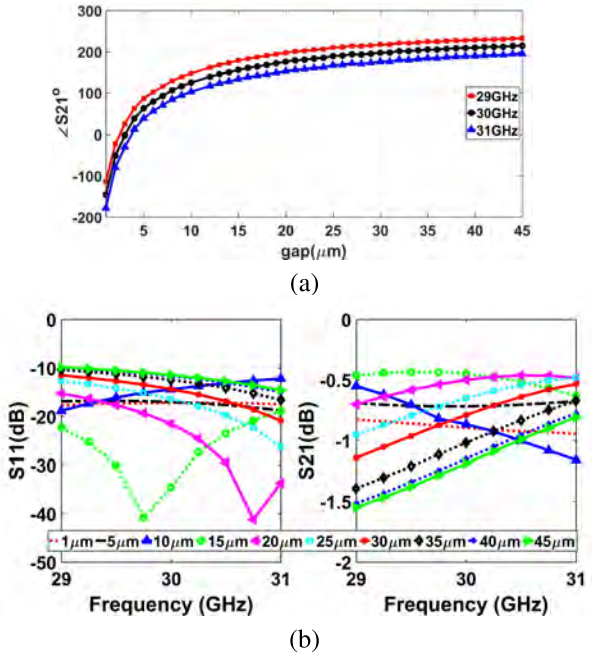

Fig. 6. Simulated results for proposed phase shifter for different h_{gap}. (a) Phase versus h_{gap}. (b) S-parameters versus frequency.

B. Low-Profile Magnetic Actuator

One of the most challenging aspects to loading a transmission line with a dielectric slab in order to realize a phase shifter is the actuation technique. Existing solutions [29], [30], [32]–[35], such as PET, have a high profile, high driving voltages, and high fabrication costs. To overcome these limitations, a high-performance, low-cost, and low-profile actuation mechanism is introduced in this paper. The proposed actuation mechanism consists of an integrated miniaturized permanent magnet made from materials with high magnetization such as samarium-cobalt (SmCo) and a planar magnetic coil. The proposed magnetic actuator utilizes the repulsion and attraction forces occurring between the permanent magnet and the planar magnetic coil to move the BLT slab with high precision and in the most repeatable manner. The BLT slab is attached to a flexible polyimide membrane supported by two beams to keep the BLT slab in its proper position during actuation. The polyimide membrane has a 50 μm thickness, a beamwidth of $W_b = 200$ μm, a gap of $G_b = 200$ μm, a 2×4 mm^2 base on which to attach the BLT slab, and a 1.1 mm opening to hold the SmCo magnet, as shown in Fig. 7(a). A very thin SmCo magnet (typically considered to have a thickness and diameters $<$ 1 mm),

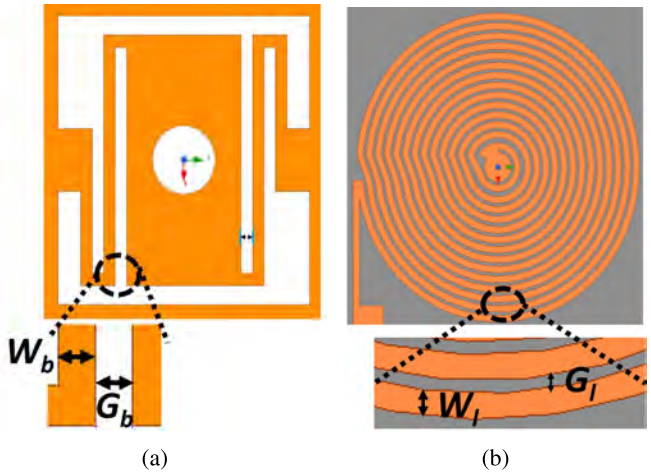

Fig. 7. Proposed polyimide membrane and planar electromagnetic coil. (a) Top view of polyimide membrane. (b) Top view of planar magnetic coil.

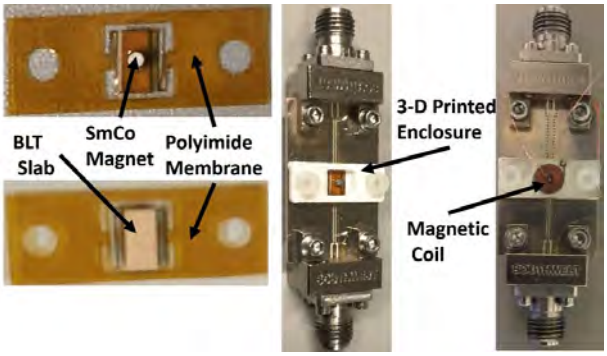

Fig. 8. Fabricated phase shifter's circuit and actuator components.

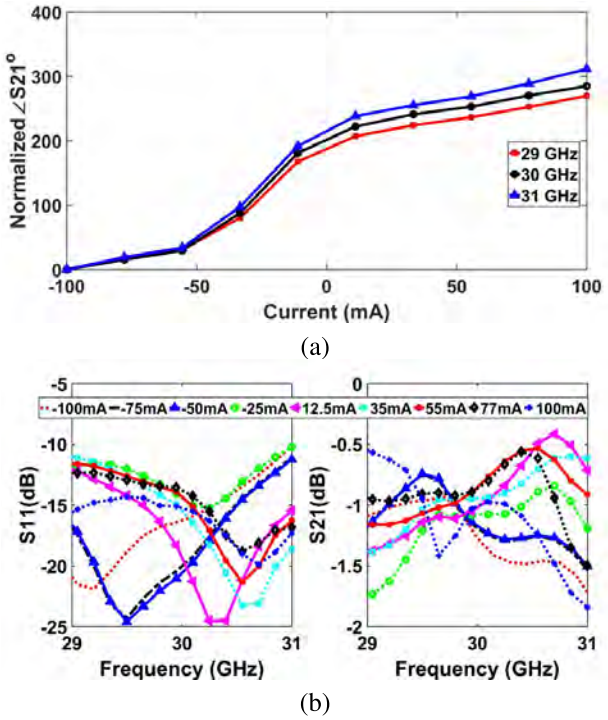

Fig. 9. Measured results for proposed phase shifter for different applied currents. (a) Normalized phase versus applied current. (b) S-parameters versus frequency.

is placed on the top of the polyimide membrane. A tunable current source is employed to control the current of the magnetic coil thus generating an adjustable and reversible magnetic force. The magnetic coil was implemented on an FR4 PCB substrate with a spiral shape. A typical design has a linewidth of $W_l = 100$ μm, a gap between turns of $G_l = 50$ μm, and 14 turns, as shown in Fig. 7(b). A 3-D printed packaging is used to enclose the proposed phase shifter and protects its components. The total height of the new actuator and its 3-D package is less than 2 mm, compared to a height of 12 mm for the PET actuator used in [29]. A field-programmable gate array-based controller is employed to precisely adjust the current so that a continuous phase shift is achieved. The proposed actuator requires only ± 40 mA to elevate the BLT slab 50 μm from the GCPW line surface; this is five times the displacement of a typical PET requiring 150 V actuation voltage.

C. Measurement Results for Proposed Phase Shifter

The proposed phase shifter was fabricated and tested using a network analyzer (PNA) from Keysight Technologies. Measurements were taken over the frequency band 29–31 GHz. Fig. 8 shows the fabricated phase shifter. The proposed phase shifting technique can provide more than 360° phase shift with proper choice of the BLT material, appropriately designed actuator, and sufficient surface smoothness. The reported structure is a proof-of-concept prototype, which can be easily improved to provide full range phase shift with minimal IL. S-parameter measurements of the proposed phase shifter demonstrated linear phase-frequency behavior with a maximum phase shift of 285° at 30 GHz when a 10 mW was applied to the magnetic actuator. The fact that the power consumption during the experiment was higher than the theoretical value is mainly due to the extra losses introduced by the interconnecting dc power lines between the magnetic coil and the current source. However, this extra power consumption can be easily eliminated by integrating the current source on top of the magnetic coil. Moreover, the proposed phase shifter was designed to achieve a 360° phase shift at 30 GHz, but measurements showed a maximum phase shift of 285°, as illustrated in Fig. 9(a). This discrepancy occurred because during simulation it was assumed that the air gap height h_{gap} could be reduced to 1 μm in order to realize the required 360° phase shift. This was not possible to achieve with the fabricated prototype mainly due to the surface roughness of the fabricated GCPW line. Such a small air gap height requires an airtight, hermetically sealed package and very smooth metallic GCPW surfaces. This type of packaging and surface characteristic will be pursued in the next phase of this paper.

Measurement results illustrate an $S_{11} < -10$ dB over the operating frequency bandwidth for different h_{gap} states, and the measured S_{11} is quite similar to the simulated result. In addition, the measurements demonstrate very low IL (S_{21}), especially at 30 GHz. They show an average S_{21} of -1 dB with an extremely low measured S_{21} variation of ± 0.2 dB

TABLE III
COMPARISON OF STATE-OF-THE-ART PASSIVE PHASE SHIFTERS

Reference	[32]	[33]	[34]	[35]	This work
Perturber type	Metallic slab	Low dielectric slab	Low dielectric slab	magneto dielectric	High dielectric slab
Frequency (GHz)	6	9.7	6	20	30
$\Delta\phi^o_{max}$	860	132	60	384	285
$\lvert IL_{max}\rvert$ (dB)	3.80	2.31	1.00	4.50	1.20
$FOM = \frac{\Delta\phi^o_{max}}{\lvert IL_{max}\rvert}$	212	57	60	85.3	237.5
Area (mm^2)	12.8×12.8	73×32	7×3.18	12×4	4×2
Packaged	No	No	No	No	Yes
Actuation	PET	PET	PET	PET	Magnetic actuator
Power consumption	High	High	High	High	Low

around the center frequency (30 GHz). The measured IL is one of the best reported to-date in the literature (see Table III). Fig. 9(b) presents the measured S-parameters versus frequency for the proposed phase shifter at different applied current states. Table III compares the performance of the phase shifter presented here with state-of-the-art phase shifters that use similar phase shifting mechanisms.

IV. 1×4 MM-WAVE PASSIVE PHASED-ARRAY ANTENNA

The proposed phase shifter and CP antenna were integrated to construct a proof-of-concept 1×4 passive PAA to operate at the mm-W frequency range (29.5–30.5 GHz). It consists of four CP antenna elements arranged in a linear grid, four phase shifters, and a corporate feeding network. In the proposed structure, since each antenna element has a phase shifter, which can be controlled independently, the beam can be steered in two directions off-boresight and the proposed phase shifting mechanism not only able to compensate for substrate warpage but also for other mechanical and fabrication errors which are inevitable. Therefore, accurate and flexible beam scanning can be achieved over the angles ranging from $-90°$ to $+90°$ in elevation—an advantageous feature of the proposed passive PAA over the existing solutions [18]–[26]. The proposed array was fabricated on a 4000 series three-layer PCB from Rogers Corporation. A 5 mm ($0.5\ \lambda_o$) interelement spacing was used. The proposed passive PAA was simulated for different scanning angles over the frequency band of interest.

A. Measurement and Simulation Results for Proposed 1×4 mm-Wave Passive Phased-Array Antenna

A PNA was used to measure the reflection coefficient (S_{11}) of the fabricated passive PAA. The antenna shows

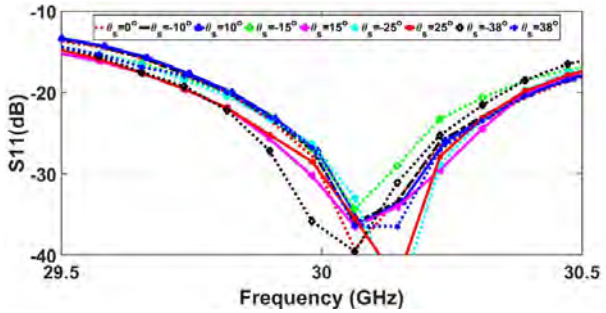

Fig. 10. Measured reflection coefficient at different steering angles.

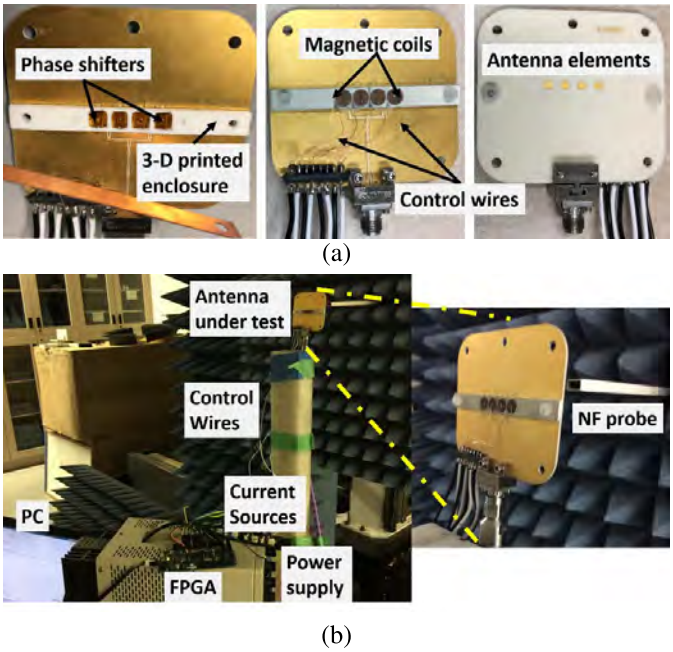

Fig. 11. Measurement setup. (a) Fabricated passive PAA. (b) PNF measurement setup.

a $S_{11} < -10$ dB over the operating frequency band for all steering angles with small variations as shown in Fig. 10. A planar near-field (PNF) measurement system from NSI was used to measure the radiation characteristics of the passive PAA. The measurement setup is illustrated in Fig. 11. A lookup table was extracted for each phase shifter by employing the NF system probe. The probe was placed very close to each antenna element and by varying the current source the phase range could be obtained for each individual antenna element. The extracted data were saved as a lookup table. The theoretical basis of this calibration method is introduced in [36]. The look-up tables were loaded to a PC and the array factor theory was used to calculate the required progressive phase to steer the beam of the antenna under test toward different elevation angles. The maximum realized phase shift was 320°, when a 100 mA current was applied to the magnetic coil. The proposed 1×4 passive PAA prototype consumes maximally 40 mW dc power.

The passive PAA was tested over the frequency band (29–31 GHz). Its measured results were compared to the

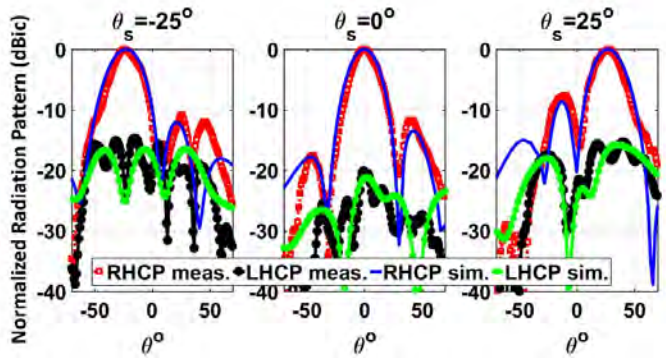

Fig. 12. Measured and simulated radiation patterns at 30 GHz for different steering angles.

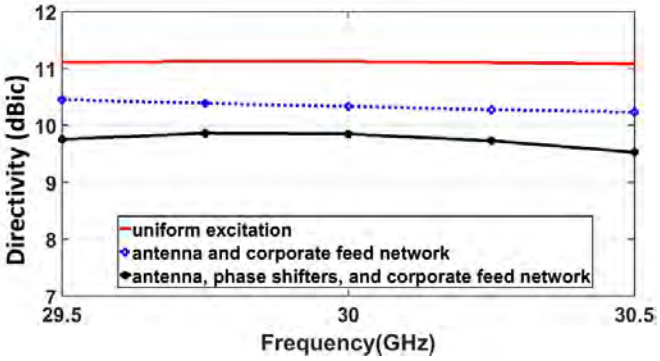

Fig. 13. Simulated directivity for three different cases: uniform excitation; antenna and corporate feed network; and proposed concept passive PAA.

simulated results for three different steering angles at 30 GHz. A right-hand CP (RHCP) beam was realized with high cross-polarization discrimination. Measurements showed a 20 dB cross-polarization discrimination at boresight that agrees with what the simulation results had predicted; furthermore, $<$ 11 dB sidelobe level (SLL) was found by both measurement and simulation analyses. In addition, the measured results agree with those found through simulation for the $\pm 25°$ steering angles, as shown in Fig. 12.

For completeness, the NF system was used to measure the directivity and gain of the antenna under test. The standard method consists of two steps: 1) measuring the directivity from the scanned data and 2) using a standard gain horn antenna to calibrate the NF system. The antenna gain is then obtained from the measured directivity and the standard gain measurement. The radiation efficiency (= gain/directivity) can be calculated from these measurements as well.

The simulated directivity of the proposed 1×4 passive PAA is 9.874 dBic at 30 GHz. Part of the reduction in the directivity is attributed to mutual coupling and different environment of the two edge elements as compared to those of the two internal elements. Moreover, it is found that due to the cooptimization of the corporate feeding network with antennas and BLT phase shifters, the power splitter introduced unbalanced amplitude and phase to the antenna elements. The internal two elements receive more power as compared to the two edge elements with 30° phase difference. The resulting amplitude tapering, which becomes intensified when the BLT phase shifters are introduced into the feeding network. Accordingly, the directivity of the 1×4 passive PAA is reduced. Full-wave simulations were performed to verify this conclusion. Fig. 13 depicts the simulated directivity for three different cases, namely, ideal uniform excitation, antenna and corporate feed network, and proposed feed circuit containing BLT phase shifters. If the antenna elements are excited independently with the same amplitude and phase, an 11.12 dBic directivity is realized at 30 GHz. If we excite the four antenna elements by the developed corporate feeding network without BLT phase shifters; the simulated directivity at 30 GHz is 10.34 dBic. Finally, integrating the BLT-based phase shifters with the 1×4 antenna array (passive phased array configuration) leads to a simulated directivity of 9.85 dBic at 30 GHz. As a result, as compared to the uniform excitation case, a 1.27 dBi directivity reduction occurred due to the above-mentioned factors. This issue will be resolved in the next phase of this paper where a larger and a better optimized array will be developed.

TABLE IV
SUMMARY OF MEASURED 1×4 CP PASSIVE PAA AT 30 GHz

	29.5 GHz								
θ_s^o	-38^o	-25^o	-15^o	-10^o	0^o	$+10^o$	$+15^o$	$+25^o$	$+38^o$
X-Pol discrimination(dB)	22	16	16.3	18.6	19	19	18.8	15.8	19.3
1^{st}SLL (dB)	6	9.7	8.7	9.6	11.9	10.6	7.6	7	4.4
	30 GHz								
X-Pol discrimination(dB)	23	22.5	20.4	18.4	20.33	22	18.4	17.9	15.85
1^{st}SLL (dB)	7	10.9	7.2	9	11.75	11.9	7.6	7.6	3.7
	30.5 GHz								
X-Pol discrimination(dB)	19.4	15	18.7	18.3	23	20.7	20.2	16	20.7
1^{st}SLL (dB)	8.35	16.5	6	9.7	12.1	13.5	8	7.8	3.8

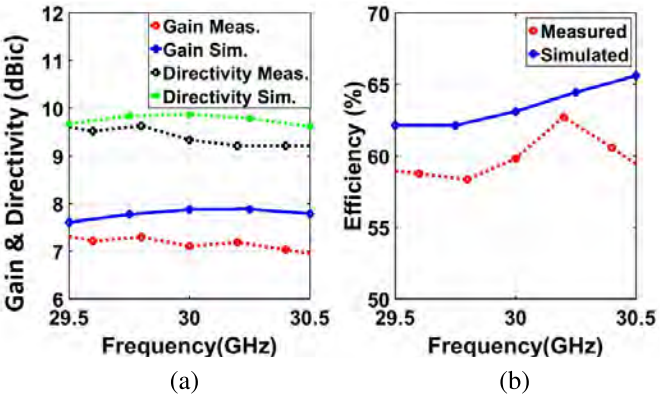

(a) (b)

Fig. 14. Measured and simulated gain, directivity, and radiation efficiency. (a) Gain and directivity. (b) Radiation efficiency.

The maximum measured gain was 7.4 dBic with 0.5 dB variation. The maximum measured directivity was 9.75 dBic with 0.5 dB variation over the operating frequency band for the boresight case. A good correlation was observed between the measured and simulated gain, and between the measured and simulated directivity, as shown in Fig. 14(a). The passive PAA shows a measured radiation efficiency of 60% at 30 GHz—exceptional performance for a passive PAA system. To the best of the authors' knowledge, no similar performance had been reported in the literature. The measured and simulated radiation efficiencies are depicted in Fig. 14(b).

TABLE V
COMPARISON OF STATE-OF-THE-ART PASSIVE PAA

Reference	[18]	[20]	[22]	[23]	[25]	[26]	This work
Frequency (GHz)	16	33	30	15	35	60	30
Scanning coverage	1-D	1-D	1-D	1-D	1-D	1-D	1-D
Measured scanning range	$0^o - +30^o$	$-21^o - +24^o$	$-17^o - +19^o$	$0 - +25^o$	$0 - +33^o$	$-1.6^o - +2.9^o$	$-38^o - +38^o$
Polarization	LP	LP	LP	LP	LP	LP	CP
Measured gain (dB)	-	-	-	8	15.6	15	7.4
Efficiency (%)	-	-	-	-	-	39.9	60
Profile	High	High	High	High	High	High	Low
Array size	1×4	1×8	1×8	1×8	1×4	4×4	1×4
Voltage range (V)	0-60	0-50	0-40	0-60	0-60	0-100	0-0.1
Actuation	PET	PET	PET	PET	PET	PET	Magnetic actuator
Packaged	No	No	No	No	No	No	Yes

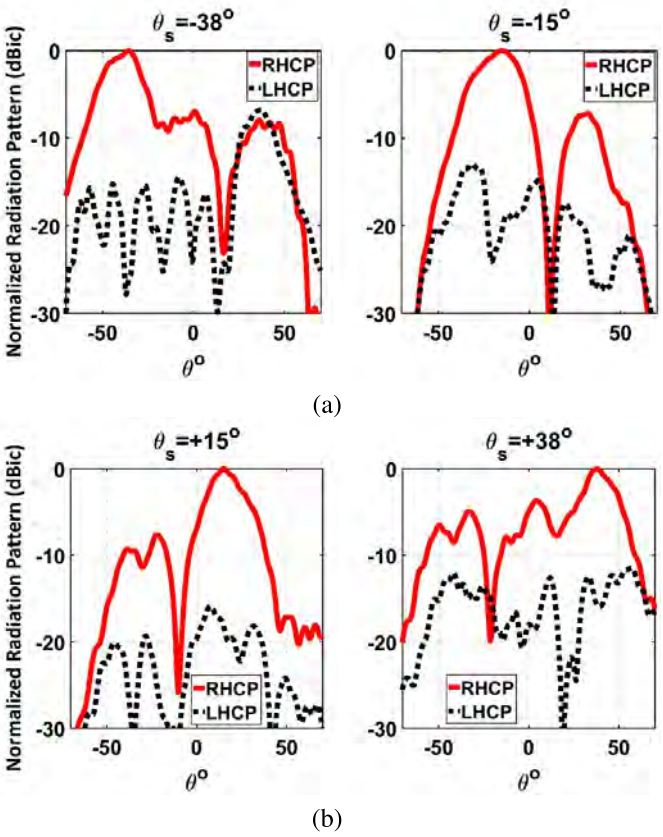

Fig. 15. Measured RHCP (Co-Pol) and LHCP (X-Pol) patterns at 30 GHz. (a) $-38°$ and $-15°$. (b) $+15°$ and $+38°$.

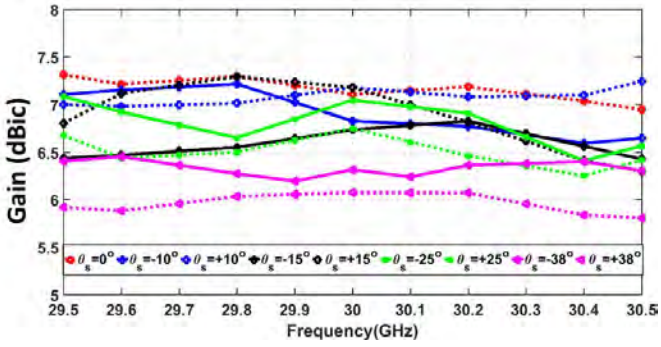

Fig. 16. Measured gain at different steering angles.

B. Measurement Summary

The proposed passive PAA was tested for different steering angles in elevation to validate its performance and capabilities. The main beam was steered toward the angles (0°, ±10°, ±15°, ±25°, and ±38°), and it demonstrated an RHCP beam with low pointing error $<2°$ in all cases over the frequency bandwidth 29.5–30.5 GHz with an AR $<$ 3 dB. Fig. 15(a) and (b) illustrates the measured RHCP and LHCP components of the proposed passive PAA. It can be observed that the main beam was properly formed in all steering angles. The proposed phased array maintains good CP and high cross-polarization discrimination over a 1 GHz frequency band centered at 30 GHz, with excellent beam pointing and acceptable SLLs. The proposed passive phased array demonstrates a gain variation, $\sim$ 1 dB at 30 GHz, for different steering angles. This gain variation is due to the scanning loss, as shown in Fig. 16. Theoretically, the SLLs for any θ_s should be the same. However, due to the limited number of calibration points, the phase shifters characterization in this initial stage of research was not very accurate and most of the calibration data over the entire phase shift range were obtained by interpolation over a limited number of measurements (10 points per each phase shifter). This inaccuracy led to asymmetry in the measured gain and SLLs. Table IV summarizes the radiation characteristics of the proposed passive PAA at 30 GHz for different scanning angles.

Finally, an extensive comparison between the presented passive PAA and state-of-the-art passive PAAs is given in Table V. This comparison focuses on aspects that are the most critical factors in designing an efficient and low-cost passive PAA suitable for implementation in a large-scale system.

V. Conclusion

In this paper, the process of developing and successfully fabricating a novel *Ka*-band CP passive PAA was presented, along with measurement results. To the best of the authors' knowledge, it is the first time that a multiantenna module, employing a BLT-based phase shifter circuit, has been introduced for used in a CP passive PAA with full electronic control of each individual antenna element. The proposed system was implemented using a low-cost PCB technology. A low-profile and efficient magnetic actuator was proposed and utilized to control the phase shifter. A wide scanning angle ($\pm 38°$) was achieved with high precision. Given these results, the presented module is suitable for large-scale mm-W PAA systems with full electronic beam control capabilities toward any azimuth and elevation. The proposed structure will be extended to a 2-D CP passive PAA for emerging mm-W applications, which require low-profile, low-cost, and low-power consumption systems with full beam control capability.

References

[1] Q. Luo *et al.*, "Design and analysis of a reflectarray using slot antenna elements for Ka-band SatCom," *IEEE Trans. Antennas Propag.*, vol. 63, no. 4, pp. 1365–1374, Apr. 2015.

[2] Q. Luo, S. Gao, and L. Zhang, "Millimeter-wave smart antennas for advanced satellite communications," in *Proc. IEEE MTT-S Int. Microw. Symp. (IMS)*, May 2015, pp. 1–4.

[3] J. S. Silva, E. B. Lima, J. R. Costa, C. A. Fernandes, and J. R. Mosig, "Tx-Rx lens-based satellite-on-the-move Ka-band antenna," *IEEE Antennas Wireless Propag. Lett.*, vol. 14, pp. 1408–1411, 2015.

[4] C. I. Kourogiorgas, P. D. Arapoglou, and A. D. Panagopoulos, "Statistical characterization of adjacent satellite interference for earth stations on mobile platforms operating at Ku and Ka bands," *IEEE Wireless Commun. Lett.*, vol. 4, no. 1, pp. 82–85, Feb. 2015.

[5] S. Vaccaro, L. Diamond, D. Runyon, and M. C. Vigano, "Ka-band mobility terminals enabling new services," in *Proc. 8th Eur. Conf. Antennas Propag. (EuCAP)*, Apr. 2014, pp. 2617–2618.

[6] T. Chaloun *et al.*, "Wide-angle scanning active transmit/receive reflectarray," *IET Microw., Antennas Propag.*, vol. 8, no. 11, pp. 811–818, Aug. 2014.

[7] S. Kutty and D. Sen, "Beamforming for millimeter wave communications: An inclusive survey," *IEEE Commun. Surveys Tuts.*, vol. 18, no. 2, pp. 949–973, 2nd Quart., 2016.

[8] R. Bonjour *et al.*, "Ultra-fast millimeter wave beam steering," *IEEE J. Quantum Electron.*, vol. 52, no. 1, Jan. 2016, Art. no. 0600708.

[9] Z. Cao *et al.*, "Advanced integration techniques on broadband millimeter-wave beam steering for 5G wireless networks and beyond," *IEEE J. Quantum Electron.*, vol. 52, no. 1, Jan. 2016, Art. no. 0600620.

[10] J. Helander, K. Zhao, Z. Ying, and D. Sjöberg, "Performance analysis of millimeter-wave phased array antennas in cellular handsets," *IEEE Antennas Wireless Propag. Lett.*, vol. 15, pp. 504–507, 2016.

[11] S. Sun, T. S. Rappaport, R. W. Heath, Jr., A. Nix, and S. Rangan, "MIMO for millimeter-wave wireless communications: Beamforming, spatial multiplexing, or both?" *IEEE Commun. Mag.*, vol. 52, no. 12, pp. 110–121, Dec. 2014.

[12] S. B. Yeap, X. Qing, and Z. N. Chen, "77-GHz dual-layer transmitarray for automotive radar applications," *IEEE Trans. Antennas Propag.*, vol. 63, no. 6, pp. 2833–2837, Jun. 2015.

[13] M. Imbert, A. Papió, F. De Flaviis, L. Jofre, and J. Romeu, "Design and performance evaluation of a dielectric flat lens for millimeter-wave applications," in *Proc. 8th Eur. Conf. Antennas Propag. (EuCAP)*, Apr. 2014, pp. 3193–3196.

[14] M. Gachev, V. Boyanov, S. Kamenopolsky, V. Peshlov, B. Marinov, and P. Dankov, "On-the-move antenna systems for broad-band satellite communications," in *Proc. 8th Eur. Conf. Antennas Propag. (EuCAP)*, Apr. 2014, pp. 3193–3196.

[15] S. Borisov and A. Shishlov, "Antennas for satcom-on-the-move, review," in *Proc. Int. Conf. Eng. Telecommun. (EnT)*, Nov. 2014, pp. 3–7.

[16] H. Zhou, M. Jong, and G. Lo, "Evolution of satellite communication antennas on mobile ground terminals," *Int. J. Antennas Propag.*, vol. 2015, Jul. 2015, Art. no. 436250.

[17] Y. Rahmat-Samii and A. C. Densmore, "Technology trends and challenges of antennas for satellite communication systems," *IEEE Trans. Antennas Propag.*, vol. 63, no. 4, pp. 1191–1204, Apr. 2015.

[18] S.-G. Kim and K. Chang, "Ultra wideband 8 to 40 GHz beam scanning phased array using antipodal exponentially-tapered slot antennas," in *IEEE MTT-S Int. Microw. Symp. Dig.*, vol. 3, Jun. 2004, pp. 1757–1760.

[19] C.-C. Chang, C. W. Domier, and N. Luhmann, "Microwave beam focusing/shaping phased antenna arrays," in *IEEE MTT-S Int. Microw. Symp. Dig.*, vol. 3, Jun. 2004, pp. 1765–1768.

[20] L. Yang, C. W. Domier, and N. C. Luhmann, "Ka-band true time delay e-plane beam scanning and broadening phased array system using antipodal elliptically-tapered slot antennas," in *Proc. IEEE Antennas Propag. Soc. Int. Symp.*, Jul. 2006, pp. 2213–2216.

[21] L. Yang, N. Ito, C. W. Domier, N. C. Luhmann, Jr., and A. Mase, "20 to 40 GHz beam shaping/steering phased antenna array system using Fermi tapered slot antennas," in *IEEE MTT-S Int. Microw. Symp. Dig*, Jun. 2007, pp. 1887–1890.

[22] L. Yang, N. Ito, C. W. Domier, N. C. Luhmann, and A. Mase, "18–40-GHzBeam-shaping/steering phased antenna array system using Fermi antenna," *IEEE Trans. Microw. Theory Techn.*, vol. 56, no. 4, pp. 767–773, Apr. 2008.

[23] D.-J. Jung, C. H. Kim, and K. Chang, "Broadband 8 to 18 GHz phased array system for communications," in *Proc. Asia Pacific Microw. Conf. (APMC)*, Dec. 2012, pp. 406–408.

[24] M. A. Ashraf, S. Alshebeili, M. Alkanhal, and A. R. Sebak, "Ultra wideband phased array antenna using slow wave microstrip dielectric loaded phase shifters," in *Proc. 16th Int. Symp. Antenna Technol. Appl. Electromagn. (ANTEM)*, Jul. 2014, pp. 1–2.

[25] Y. Zhang, J. Bai, S. Shi, and D. W. Prather, "Ka-band phased patch array antenna integrated with a PET-controlled phase shifter," *Int. J. RF Microw. Comput.-Aided Eng.*, vol. 26, no. 3, pp. 199–208, Mar. 2016.

[26] Z. Briqech, A.-R. Sebak, and T. A. Denidni, "Low-cost wideband mm-wave phased array using the piezoelectric transducer for 5G applications," *IEEE Trans. Antennas Propag.*, vol. 65, no. 12, pp. 6403–6412, Dec. 2017.

[27] H. Al-Saedi, W. Abdel-Wahab, S. M. Raeis-Zadeh, S. Gigoyan, and S. Safavi-Naeini, "A wide axial ratio beamwidth circularly polarized antenna for Ka-band satellite on the move (SOTM) phased array applications," in *Proc. IEEE Int. Symp. Antennas Propag. USNC/URSI Nat. Radio Sci. Meeting*, Jul. 2017, pp. 2557–2558.

[28] N. Kumprasert, "Theoretical study of dual-resonant frequency and circular polarization of elliptical microstrip antennas," in *Proc. IEEE Antennas Propag. Soc. Int. Symp.*, vol. 2, Jul. 2000, pp. 1015–1020.

[29] H. Al-Saedi, W. M. Abdel-Wahab, S. Gigoyan, A. Taeb, and S. Safavi-Naeini, "A low-cost wideband phase shifter for two-way mm-wave phased array antenna system," *Int. J. Microw. Wireless Technol.*, vol. 10, no. 1, pp. 77–86, 2018.

[30] A. S. Abdellatif *et al.*, "Low loss, wideband, and compact CPW-based phase shifter for millimeter-wave applications," *IEEE Trans. Microw. Theory Techn.*, vol. 62, no. 12, pp. 3403–3413, Dec. 2014.

[31] E. A. Nenasheva and N. F. Kartenko, "High dielectric constant microwave ceramics," *J. Eur. Ceram. Soc.*, vol. 21, no. 15, pp. 2697–2701, 2001.

[32] J. Wu *et al.*, "Compact, low-loss, wideband, and high-power handling phase shifters with piezoelectric transducer-controlled metallic perturber," *IEEE Trans. Microw. Theory Techn.*, vol. 60, no. 6, pp. 1587–1594, Jun. 2012.

[33] C. H. Kim and K. Chang, "A reflection-type phase shifter controlled by a piezoelectric transducer," *Microw. Opt. Technol. Lett.*, vol. 53, no. 4, pp. 938–940, 2011.

[34] S.-G. Kim, T.-Y. Yun, and K. Chang, "Time-delay phase shifter controlled by piezoelectric transducer on coplanar waveguide," *IEEE Microw. Wireless Compon. Lett.*, vol. 13, no. 1, pp. 19–20, Jan. 2003.

[35] G. M. Yang and N. X. Sun, "Tunable ultrawideband phase shifters with magnetodielectric disturber controlled by a piezoelectric transducer," *IEEE Trans. Magn.*, vol. 50, no. 11, pp. 1–4, Nov. 2014.

[36] P. W. Hannan and M. A. Balfour, "Simulation of a phased-array antenna in waveguide," *IEEE Trans. Antennas Propag.*, vol. AP-13, no. 3, pp. 342–353, May 1965.

Hussam Al-Saedi (S'14) received the B.Sc. degree in electrical engineering from the University of Technology, Iraq, Baghdad, Iraq, in 2005, the M.Sc. degree in electronic engineering from the Politecnico Di Torino, Turin, Italy, in 2010, and the Ph.D. degree in electrical engineering from the University of Waterloo, Waterloo, ON, Canada, in 2018.

From 2010 to 2013, he was a Lecturer Assistant with the Department of Electrical Engineering, University of Technology, Iraq. He is currently a Faculty Member with the Department of Communication Engineering, University of Technology, Iraq. He is also a Research Assistance with the Center for Intelligent Antenna and Radio System, University of Waterloo. He has coauthored 10 peer-reviewed journal papers and 35+ peer-reviewed international conference papers. His current research interests include wideband and wide-beam-steering millimeter-wave (mm-W) [active phased-array antennas, passive phased-array antennas, and steerable reflectarray antennas] for Emerging *Ka*-band mobile satellite communications and 5G wireless communications, mm-W switchable circularly polarized antennas with high polarization purity, ultrawideband mm-W phased shifters, and metal only reflectarray antennas.

Suren Gigoyan received the M.S. degree from the Physics Department, Yerevan State University, Yerevan, Armenia, in 1980, and the Ph.D. degree in electrical engineering from the Institute of Electrical Engineering, Moscow, Russia, in 1991.

From 2005 to 2006, he was a Visiting Fulbright Scholar with the University of Tennessee, Knoxville, TN, USA. He is currently a Visitor Scientist with the Center for Intelligent Antenna and Radio System, University of Waterloo, Waterloo, ON, Canada. He has authored/coauthored more than 70 peer-reviewed journal and conference papers. His current research interests include millimeter and THz spectroscopy, submillimeter frequency range devices and system design, application of MEMS structures in THz spectroscopy, sensing, cancer, and DNA detection.

Wael M. Abdel-Wahab received the M.S. degree in RF-microwave engineering and antennas from the Department of Electronics and Electrical Communications Engineering, Cairo University, Giza, Egypt, in 2004, and the Ph.D. degree in RF-microwave engineering and antennas from the Department of Electrical and Computer Engineering, University of Waterloo, Waterloo, ON, Canada, in 2011.

From 2011 to 2013, he was a Cross-Appointed Post-Doctoral Fellow with the Department of Electrical and Computer Engineering, University of Waterloo, and the Department of Electrical, Computer, and Software Engineering, University of Ontario Institute of Technology, Oshawa, ON, Canada. He is currently a Research Assistant Professor with the Centre for Intelligent Antenna and Radio Systems, Electrical and Computer Engineering, University of Waterloo. Since 2014, He has been with C-COM Satellite System Inc., Ottawa, ON, Canada, as a Senior RF/Antenna Engineer for research and development. He has authored/coauthored more than 50 research papers in highly cited journals and conferences in RF/microwave circuits and antennas. His current research interests include low cost millimeter-wave phased array antennas and RF-circuits for the new emerging Mobile Satellite Communication and 5G technologies.

Dr. Abdel-Wahab served as a reviewer for the IEEE Antennas and Propagation Society's journals such as the IEEE TRANSACTION ON ANTENNA AND PROPAGATION and IEEE ANTENNA AND WIRELESS LETTERS, and IET Society's Journals such as *IET Microwave, Antennas & Propagation* and *Electronic Letters*. He was a recipient of many prestigious awards, such as the Ph.D. Egyptian Scholarship in 2006, the Ontario Ministry of Economic Development and Innovation Fellowship in 2011, the Natural Science and Engineering Research Council of Canada Visiting Fellowship in Canadian Government Laboratories Program in 2014 (declined), and the Industrial Research Assistance Program Fellowship funded by National Research Council of Canada during the period from 2014 to 2016.

Ardeshir Palizban received the B.Sc. degree in electrical engineering (telecommunication) from Tehran University, Tehran, Iran, in 1988.

He was a Research Engineer with the Iran Telecommunication Research Center, Tehran, where he was involved in digital multiplexer and optical communication systems. He was the Technical Manager with Payke Vaset Engineering Company, Tehran, for the design of digital and analog studio equipment and fiber optic communication systems and supervisory systems. He is currently a Research Associate with the Centre for Intelligent Antenna and Radio Systems Group, University of Waterloo. He is involved in the active and passive phased array systems, especially hardware and software design of electronic subsystem of the array. His current research interests include low-cost phase array calibration system, active and passive phased array, piezoelectric actuator and low-profile precise current source.

Aidin Taeb (M'14) received the B.Sc. degree in electrical engineering from Tabriz University, Tabriz, Iran, in 2003, the M.Sc. degree in electromagnetic and antennas from the Amirkabir University of Technology (Tehran Polytechnique), Tehran, in 2006, the Ph.D. degree from the University of Waterloo, Waterloo, ON, Canada, in 2015. His doctoral dissertation was on the development of a new silicon-based technology for millimeter-wave (mm-W) and terahertz (THz) integrated systems.

He is currently a Research Associate with the Centre for Intelligent Antenna and Radio Systems (CIARS) Group, University of Waterloo. He is currently investigating the new generation of integrated sub mm-W and THz technology. He is a Lead Engineer in the field of mm-W/THz and antenna measurement with CIARS. His current research interests include mm-W/THz bio-sensors, especially DNA and protein sensors, design of satellite antennas, mm-W cancer detector, and mm-W/THz silicon on-chip/in-package circuits.

Ahmad Ehsandar received the B.Sc. degree in mechanical engineering from the Sharif University of Technology, Tehran, Iran, in 2006, the M.Sc. degree in biomechanical engineering from the Amirkabir University of Technology, Tehran, in 2010, and the Ph.D. degree from the University of Waterloo, Waterloo, ON, Canada, in 2015.

In 2015, he joined the Centre of Intelligent Antenna and Radio Systems Group, University of Waterloo, as a Research Associate, where he was involved in the development of various millimeter-wave, terahertz, and optic projects. He was involved in the design of heat-efficient PCB packages, low profile heatsink for electronic cooling, and the performance of thermal analysis for electromechanical assemblies. Since 2015, he has been the Lead Mechanical Engineer, Centre for Intelligent Antenna and Radio Systems, University of Waterloo, where he is involved in the design and prototype of the low-profile satellite-on-the-move phased array project funded by Natural Science and Engineering Research Council and C-COM Satellite Inc.

Elizaveta Nenasheva received the M.Sc. and Ph.D. degrees in physics from Saint Petersburg Electrotechnical University, St. Petersburg, Russia, in 1974 and 1981, respectively.

She was the In-Charge of the Department of Microwave Ceramics, Giricond Research Institute, St. Petersburg. She was the Head of Research and Industrial Complex, High Frequency Ceramic Materials and Microwave products, Giricond Research Institute. She is currently a Visiting Professor with the HEP Division, Argonne National Laboratory, Chicago, IL, USA, and a Visiting Senior Researcher with Euclid Techlabs LLC, Washington, DC, USA, where she was involved in various DOE SBIR grant programs funded by the U.S. Department of Energy. She is also the Director of Ceramics Co. Ltd., Private R&D Company, St. Petersburg. She has authored/coauthored more than 140 papers in the field of microwave ceramic and smart materials development. She holds 51 national and international patents in the field of microwave ceramics compositions and ferroelectric technology development.

Dr. Nenasheva is a member of the International Advisory Board of the microwave materials and their applications.

Safieddin Safavi-Naeini (LF'17) received the B.Sc. degree in electrical engineering from the University of Tehran, Tehran, Iran, 1974, and the MSc. and Ph.D. degrees in electrical engineering from the University of Illinois at Urbana–Champaign, Champaign, IL, USA, in 1975 and 1979, respectively.

He is a Professor with the Department of Electrical and Computer Engineering, University of Waterloo, Waterloo, ON, Canada, where he holds NSERC/C-COM Satellite Systems Industrial Research Chair in Intelligent Radio/Antenna and Novel Electromagnetic Media. He is also the Director of the Center for Intelligent Antenna and Radio System, University of Waterloo. He has authored/coauthored 190+ journal papers and 400 conference papers in international conferences. He has led several International Collaborative Research Programs with the Research Institutes in Germany, Finland, Japan, China, Sweden, and USA. His current research interests include wide range of applications of electromagnetic devices and systems including RF/Microwave technologies, smart integrated antennas and radio systems, mm-W/THz-integrated technologies, vehicular communication systems, emerging radio technologies for intelligent transportation systems, nano-EM and photonics, EM in health science and pharmaceutical engineering, wireless communications and sensor systems and networks, new EM materials, bioelectromagnetics, biomedical instruments and computational methods.